J. Phys. D: Appl. Phys. **41** (2008) 085402 (7pp) doi:10.1088/0022-3727/41/8/085402

On the composition analysis of nc-TiC/a-C : H nanocomposite coatings

N G Chechenin[1], P N Chernykh[1], V S Kulikauskas[1], Y T Pei[2], D Vainshtein[2] and J Th M De Hosson[2]

[1] Skobeltsyn Institute of Nuclear Physics, Moscow, 119991 Russia
[2] Department of Applied Physics, Netherlands Institute for Metals Research, University of Groningen, Nijenborgh 4, 9747 AG Groningen, The Netherlands

E-mail: chechenin@sinp.msu.ru and j.t.m.de.hosson@rug.nl

Received 16 December 2007, in final form 17 January 2008
Published 6 March 2008
Online at stacks.iop.org/JPhysD/41/085402

Abstract
Using a set of ion beam analysis (IBA) techniques the compositions of hydrogenated diamond-like carbon (DLC) nanocomposite coatings are scrutinized, including the hydrogen content. The coatings are composed of two constituents: amorphous hydrocarbon matrix (a-C : H) and nanocrystalline titanium carbide (nc-TiC_a) which makes it challenging to quantify the sp^3/sp^2 ratio of the a-C : H matrix. Using IBA and SEM data, the partial mass densities of nc-TiC_a and a-C : H matrix are obtained. The latter is analysed as a function of hydrogen content and compared with the density of pure sp^3 bonding DLC and of sp^2 graphite containing different contents of hydrogen. In addition, the fraction of sp^3 bonding in the matrix is estimated assuming a linear dependence on the mass densities of the matrix.

(Some figures in this article are in colour only in the electronic version)

1. Introduction

Carbon-based coatings play an important role in modern industry due to chemical inertness, a large variety and great flexibility of electronic, optical and mechanical properties, which depend on the microstructure, the type and concentration of the additives, and the size and crystallinity of the inclusions. A large number of publications have been devoted to the detailed study of the correlation between the processing, microstructure and properties of diamond-like carbon (DLC) coatings [1]. The effect of hydrogenation on the functional properties of DLC coatings has been under debate for a long time. It is shown qualitatively that hydrogen promotes a conversion of sp^2-C to sp^3-CH bonding, resulting in an increase in the sp^3-fraction in the DLC coatings [2]. However, the problem that arises is a quantitative examination of hydrogen content, which requires a valid method of hydrogen detection. Ion beam analysis (IBA) techniques, such as nuclear reactions [3, 4] and elastic recoil detection (ERD) analysis [5–12], play a unique role in the quantitative determination of the hydrogen content. The advantage of ERD for H profiling over other techniques such as infrared (IR) and Raman spectroscopy, secondary ion mass spectroscopy (SIMS) and nuclear magnetic resonance is that it does not require a reference standard for calibration if the energy of incident ions is well below the Coulomb barrier and therefore the cross-section does not deviate significantly from the Rutherford cross-section.

In this work we have studied hydrogen containing amorphous carbon coatings with TiC nanocrystallites incorporated, nc-TiC/a-C : H. Incorporation of nanocrystalline TiC particles into the a-C : H matrix makes the DLC-based nanocomposite not only much tougher but also nearly frictionless and more wear resistant. For details on the mechanical performance and corresponding analyses refer to [13, 14]. A set of IBA techniques is used for a complete characterization of the coating composition, i.e. ERD to determine the hydrogen content, together with Rutherford backscattering (RBS) and nuclear backscattering (NBS) to characterize the concentration of carbon and heavier elements. In contrast to the expensive usage of heavy ion beam accelerators that are only available at a large facility, such as 85 MeV ^{58}Ni [9] or 11 MeV $^{12}C^{3+}$ [12], He^+ ions' beam of 2.3 MeV energy is used in this study, similar to publications in [10, 11, 15]. Here, an additional step forward is made to determine the atomic density in the coating and partial mass

density of the a-C : H matrix in a composite coating. Finally, we propose a method to estimate the sp^3 and sp^2 fractions in the matrix.

2. Coating deposition

Nanocomposite nc-TiC/a-C : H coatings were deposited via closed-field unbalanced reactive magnetron sputtering with a Hauzer HTC-1000 deposition system, which was equipped with two Cr targets and two Ti targets opposing each other as well as Ar and acetylene (C_2H_2) gas sources as described in [16]. More details of the deposition can be found in [13].

A Cr/Ti interlayer was employed to enhance the interfacial adhesion between the coating and substrate. For simplification of the composition analysis, the substrate used was a silicon wafer. The flow rate of acetylene and substrate bias varied in the range 80–125 sccm and 0–150 V, respectively, to obtain different C/Ti contents and nanostructures in the coatings. The coatings are termed xVy in such a way that the numbers before the character V indicate the substrate bias in voltage, followed by the flow rate of acetylene gas in standard cubic centimetres per minute (sccm). The thickness of the coatings (and sublayers) was examined on fracture cross sections using a scanning electron microscope (Philips FEG-XL30s) operated at ultra-high resolution (UHR) mode.

3. IBA determination of concentration of coating components

The compositions of the coatings were analysed by the IBA technique, i.e. RBS, NBS and ERD, using He^+ and H^+ ion beams with energies of 2.3 and 1.5 MeV (for NBS).

A typical RBS spectrum of nc-TiC/a-C : H coatings on the Si wafer obtained with He^+ ions of 2.3 MeV initial energy is shown in figure 1(*a*). The channel number corresponds to the energy of the detected backscattered particles. Due to the difference in the kinematic backscattering factor K, the particles backscattered by different atoms in a coating show up in different parts of the spectrum as indicated by arrows in figure 1(*a*). Figure 1(*b*) shows the deconvolution results of the RBS spectrum showing the distribution of individual elements in the coating. The step-like signals from Ti and C correspond to penetration and scattering of the particles inside the coating until overlapping with Cr signal and Si signal. The front of these latter signals is positioned in the spectrum corresponding to the thickness of the preceding layer and the K-factor values of the species. The observed extension of the signal steps is determined by the thickness of individual layers. The ramping up of Ti content and ramping down of Cr in the interlayer, as reported in [17], are clearly revealed as indicated by the arrows in figure 1(*b*).

The quantitative analysis made to fit all the IBA experimental spectra using the SIMNRA program [18] did not differ significantly from those results obtained with the RUMP [19] or DVBS [20] codes. From the fit one obtains the atomic concentrations of ith species in a jth layer:

$$c_i^j = N_i^j / N_0^j, \qquad \text{with } N_0^j = \sum_i N_i^j, \tag{1}$$

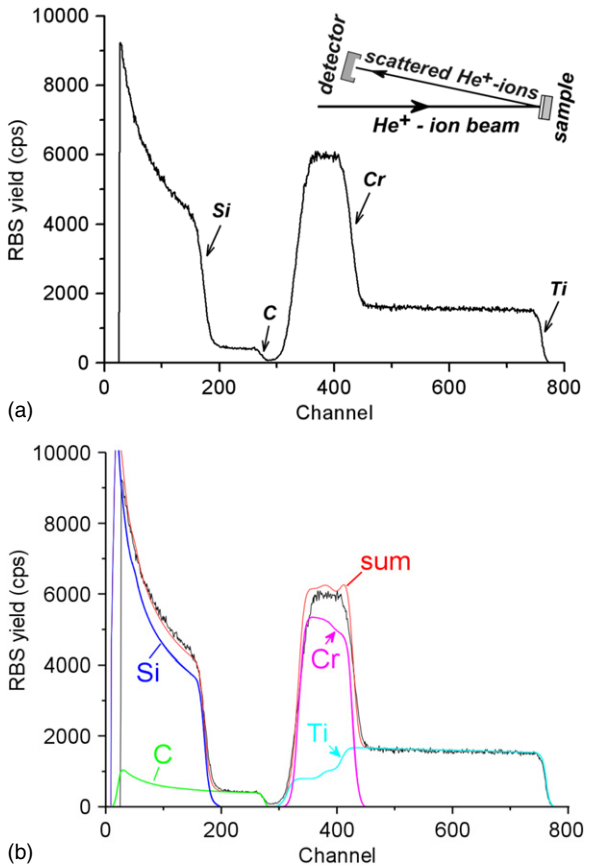

Figure 1. (*a*) RBS spectrum obtained with the He^+ beam of 2.3 MeV, with arrows indicating the front of the constituent species and an inset showing the experimental principle. (*b*) SIMNRA simulation and deconvolution of the spectrum.

where N_i^j is the partial atomic density of the ith element and N_0^j is the total atomic density in the jth layer. Inherently, the IBA methods do not give the absolute value of the volume atomic densities, but the surface atomic density ($N_i^j t_j$), where t_j is the jth layer thickness. In this paper we are concerned mostly with the top coating layer with $j = 1$ containing $C_xH_yTi_z$, on top of the CrTi interlayer. Therefore, we shall neglect the layer number symbol in short, if not mentioned otherwise.

The difference between RBS and NBS lies mainly in the backscattering cross-section, which for RBS is proportional to the squared atomic number of an element (Z^2) and therefore is smaller for lighter elements such as carbon. For protons with energy above 1 MeV the elastic backscattering cross-section can be much higher than the Rutherford cross-section due to the contribution of the nuclear elastic cross-section, giving the name the NBS analysis. Figure 2 shows a typical NBS spectrum of the same nc-TiC/a-C : H coating, where the carbon signal is much enhanced. The results of the RBS and NBS analysis were consistent within the SIMNRA treatment. Comparison of this combined IBA analysis with the electron probe micro-analysis (EPMA) measurements [13] of the titanium and carbon concentrations, in terms of their ratio, is given in figure 3. It is evidenced that the two methods are consistent with each other in the evaluation of the elements' concentrations.

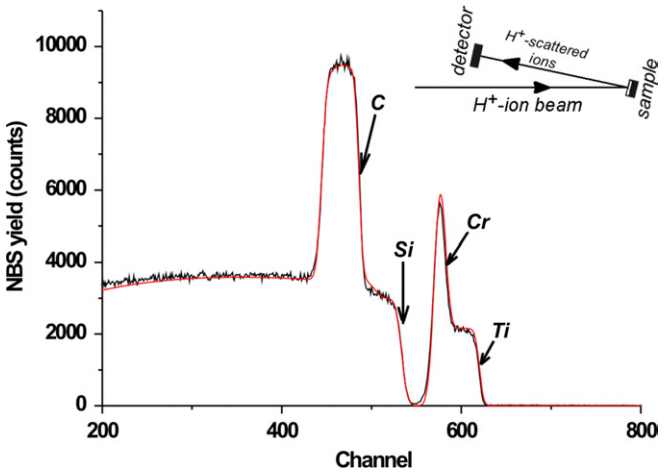

Figure 2. NBS spectrum obtained with H^+ ions of energy 1.5 MeV. A SIMNRA simulation to the coating composition of $Ti_{12}C_{57}H_{31}$ on the Si wafer with a Cr interlayer is shown together with an inset showing the experimental principle.

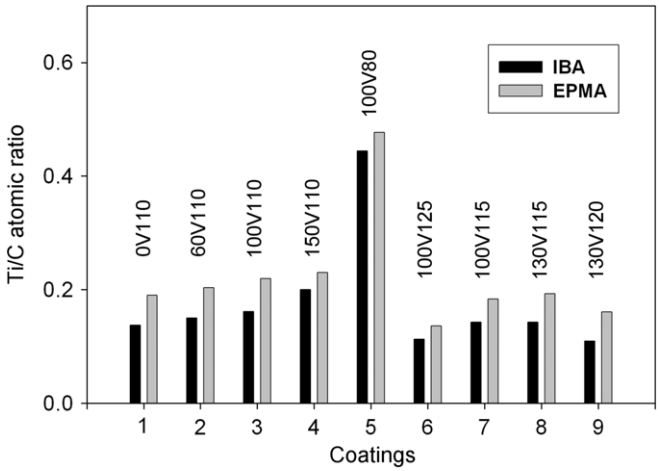

Figure 3. Comparison of Ti-to-C concentration ratios obtained using the IBA and EPMA techniques.

However, both RBS and NBS are not sensitive to hydrogen because of the kinematical restriction. The ERD technique, in contrast, can only be used to detect species lighter than the ions, i.e. hydrogen with an He^+ beam. He^+ ions of initial energy E_0 knock out H atoms with energy

$$E_{r,\max} = K E_0 = [4M_1M_2\cos^2\theta/(M_1+M_2)^2]E_0, \qquad (2)$$

where K is the kinematic factor, M_1, M_2, are the mass of incident ions and recoiled nuclei, respectively, and θ is the angle between the beam and the detector (15° in our experiment). Since He^+ ions are four times heavier than the mass of H atoms, up to 80% of the incident particle energy will be taken by the outgoing recoil nuclei. To reduce the strong background of elastically scattered He ions, a thin foil was placed in front of the semiconductor detector. Due to larger M and Z values, He ions have larger stopping power and smaller penetration in materials than H recoils. The thickness of the foil is chosen in such a way to stop only the He ions and to let the faster H ions through (2 μm Al on lavsan). The recoil

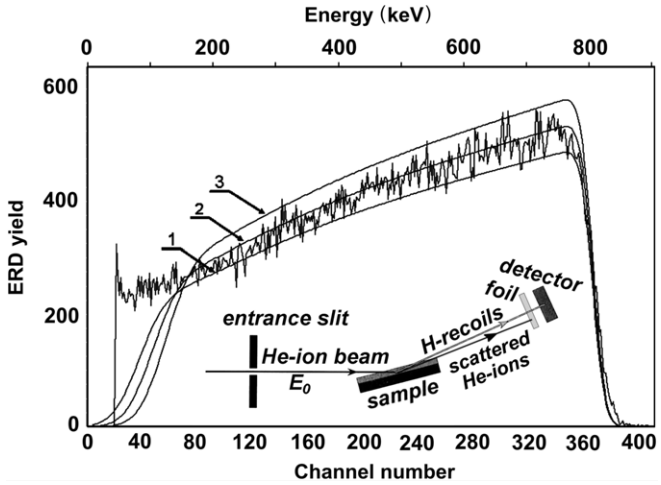

Figure 4. ERD spectrum of the coating 150V110 obtained with He^+ ions of 2.3 MeV energy and simulated curves that differ from each other by 2 at% of hydrogen. The lines demonstrate the sensitivity of the SIMNRA simulations to the concentration of hydrogen in the coating: 1—$Ti_{10}C_{64}H_{26}$; 2—$Ti_{10}C_{62}H_{28}$; 3—$Ti_{10}C_{60}H_{30}$. The experimental principle is shown in the inset.

yield is determined by the differential cross-section, which is the Rutherford recoil cross-section in laboratory frame [21]:

$$(\mathrm{d}\sigma/\mathrm{d}\Omega)_R = [Z_1Z_2e^2/(2E_0)]^2(1+M_1/M_2)^2/\cos^3\theta, \qquad (3)$$

where Z_1 and Z_2 are the atomic number of the incident ion and the recoil.

The fitting of the experimental ERD spectra was done using the SIMNRA code with hydrogen concentration N_H/N_0 as a parameter. The absolute accuracy of the H-content determination is between 5% and 10%. It is limited by the knowledge of the energy loss of He ions and H recoils and to some extent by the accuracy of the setup of the experiment geometry (see the θ dependence in equations (2) and (3)). However, for a fixed geometry of the setup and a group of samples of similar compositions, the (relative) accuracy of the H content measurements can be fairly high. In figure 4 a recorded ERD spectrum of the coating 150V110 is shown together with three curves of simulation that differ from each other by 2% in the H concentration. The comparison between the spectrum and the simulated curves clearly demonstrates that the sensitivity of the simulations is as accurate as 1% relatively to the hydrogen concentration of the coatings.

Figure 5 shows the ERD analysis results on the hydrogen concentration of the coatings as a function of the flow rate of acetylene gas and the negative bias voltage applied to the substrates during the deposition. It follows from the figure that the hydrogen concentration increases with the increase in the C_2H_2 flow rate. On the other hand, the net amount of hydrogen in the coatings decreases with increasing the bias voltage. It seems that enhanced concurrent ion impingement promotes degassing of hydrogen from the growing coating. The complete set of sample composition parameters obtained by IBA is listed in table 1.

4. Atomic density and elements depth profiling from IBA

The backscattering spectrum is used for depth profiling of species such that the scattering yield corresponds to the concentration of species and the detection channels are associated with the energy of scattered species determined by its atomic mass and the depth where the species locate. In the case of uniform distribution of elements over the thickness of a layer, the energy width of a partial contribution of the ith element in the spectrum, ΔE_i, is equal to the product of the thickness, t, of the layer in which the element is distributed, the atomic density, N_0, and the stopping power with backscattering by the species:

$$\Delta E_i = (N_0 t)[(\mathrm{d}E/\mathrm{d}x)_i/N_0], \tag{4}$$

where

$$(\mathrm{d}E/\mathrm{d}x)_i/N_0 = (K_i/\cos\theta_{\mathrm{in}})\Sigma_j[c_i\varepsilon_j(\langle E_{\mathrm{in}}\rangle)] + (1/\cos\theta_{\mathrm{out}})\Sigma_j[c_i\varepsilon_j(\langle E^i_{\mathrm{out}}\rangle)] \tag{5}$$

and $\varepsilon_j(\langle E_{\mathrm{in}}\rangle)$ and $\varepsilon_j(\langle E^i_{\mathrm{out}}\rangle)$ are specific stopping powers [22] of jth atoms for the probe ions at the average energies $\langle E_{\mathrm{in}}\rangle$ and $\langle E^i_{\mathrm{out}}\rangle$ for incoming ions into the layer and backscattered ions by ith atoms in the layer. Since the concentration of the components, $c_i = N_i/N_0$, is obtained from the IBA analysis, not only partial surface atomic density $(N_i t)$ but also total surface atomic density $(N_0 t)$ can be estimated from the partial width ΔE_i in the spectrum as follows from equations (4) and (5). In our case, the atomic surface density $(N_0 t)$ can be determined from the energy spread of the RBS Ti-signal ΔE_{Ti}, which is easily identified for the $C_xH_yTi_z$ coating as illustrated in figure 1(*a*).

If one knows N_0 then the thickness t can be obtained from $(N_0 t)$ obtained as described above. Inversely, we estimate here the thickness of a layer (t_{SEM}) with high resolution SEM cross-section observation and knowing $(N_0 t)_{\mathrm{RBS}}$ from the RBS analysis using (4) and (5); the overall atomic density N_0 can be determined from the ratio

$$N_0 = (N_0 t)_{\mathrm{RBS}}/t_{\mathrm{SEM}}. \tag{6}$$

We underline that the total atomic density N_0 for such a complicated system cannot be easily obtained by any other method. The surface densities $(N_0 t)_{\mathrm{RBS}}$ are listed in the seventh column (RBS thickness) of table 1 and N_0 values in the eighth column. The N_0 value is a useful parameter of the microstructure in many cases, for example, for evaluation of porosity. In our case it is noted that N_0 shows a decrease with increasing concentration of Ti, as demonstrated in figure 6. An evident reason for this is related to the columnar microstructure that becomes stronger with increasing Ti content [13]. It was evidenced by the transition from column-free to thicker column boundaries where a large number of atomic voids may form.

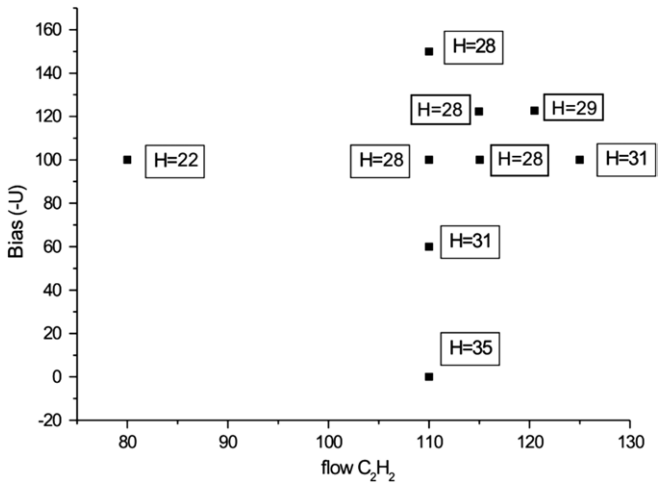

Figure 5. Hydrogen concentration (atomic percent next to the points) with errors less than 1 at% as a function of the C_2H_2 flow rate and substrate bias voltage.

5. Mass density of a-C : H matrix

Here we take a further step in expanding the area of application of IBA by suggesting a method to estimate the partial mass density of the a-C : H matrix. The composite consists of multiple phases and the averaged parameters, such as average mass density, do not give much information for understanding the physics of functional properties. It is much more inspiring to know the partial properties of the constituents of a composite, i.e. what are the properties of the precipitate and the matrix, say in the $C_xH_yTi_z$ system in particular. Assuming the top coating is homogeneous and knowing its composition by having estimated N_0 as just described, one can easily determine the mass density via multiplying N_0 by the molecular mass of the coating material.

Table 1. IBA analysis results of the composition of nc-TiC/a-C : H coatings (with $\alpha = 0.49$ in TiC_α).

Coating code	t_{SEM} (μm)	Composition (at%)				$(N_0 t)_{\mathrm{RBS}}$ ($\times 10^{19}$ at cm^{-2})	N_0 ($\times 10^{23}$ at cm^{-3})	a-C : H matrix		
		Ti	C	H	O			H content (at%)	$\rho_{\alpha=0.49}$ (g cm^{-3})	sp^3 fraction
0V110	1.14	7	51	35	7	1.35	1.18	42.3	1.42	0.06
60V110	1.24	11	58	31	—	1.42	1.15	37.0	1.64	0.19
100V110	1.16	13	59	28	—	1.30	1.12	34.7	1.67	0.16
150V110	1.17	12	60	28	—	1.38	1.18	34.1	1.78	0.27
100V80	1.06	29	49	22	—	1.15	1.08	38.7	1.84	0.49
100V125	1.37	7	62	31	—	1.66	1.21	34.6	1.74	0.24
100V115	1.19	9	63	28	—	1.40	1.18	32.3	1.78	0.22
130V115	1.15	9	63	28	—	1.35	1.17	32.3	1.77	0.21
130V120	1.17	7	64	29	—	1.45	1.24	32.4	1.73	0.17

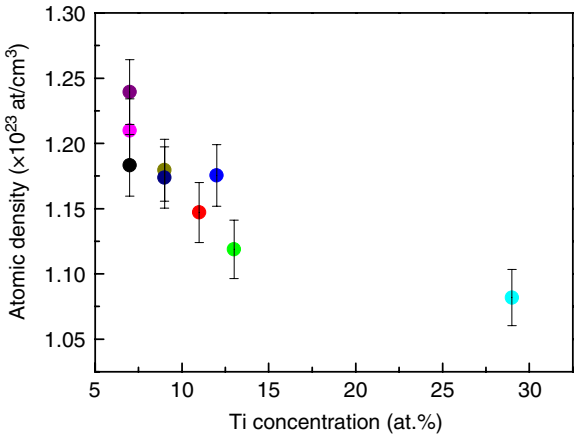

Figure 6. The atomic density N_0 of the coatings as a function of the titanium concentration.

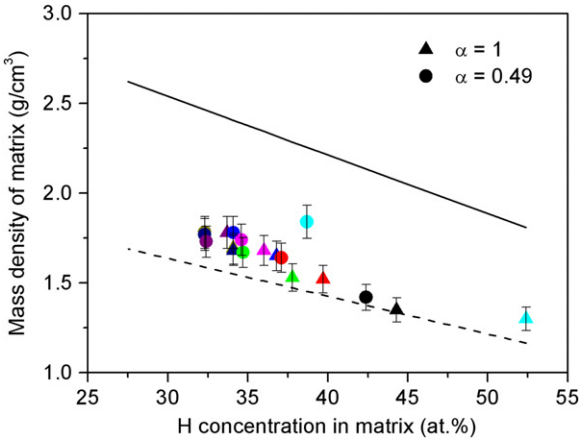

Figure 7. The mass density of the a-C : H matrix as a function of H concentration for $\alpha = 1$ (●) and $\alpha = 0.49$ (▲). The solid and dashed lines correspond to the estimates using equation (9) for the mass densities of hydrogenated diamond and graphite, respectively. Each colour of the symbols represents one coating.

To differentiate the properties of TiC precipitates from those of the matrix, one knows the partial atomic density if the total atomic density and composition of the layer are known, i.e.

$$N_0 = N_C + N_H + N_{Ti} = xN_0 + yN_0 + zN_0, \qquad (7)$$

with $x + y + z = 1$, though averaged over the layer thickness. Due to strong chemical affinity, Ti and C form a TiC compound precipitating into 2–5 nm nanocrystallites [13]. In this case, the coating can be described as a nanocomposite of TiC_α clusters embedded in the $C_{x-\alpha z}H_y$ matrix or $(TiC_\alpha)_z(CH_{y/(x-\alpha z)})_{x-\alpha z}$. The coating consists of zN_0 TiC_α quasimolecules with the molecular weight of $M_{TiC} = 47.9 + \alpha 12.01$(aem) and $(x - \alpha z)N_0$ of $CH_{y/(x-\alpha z)}$ quasimolecules with the molecular weight of $M_{CH} = 12.01 + 1(1 - x - z)/(x - \alpha z)$ (aem). The value of α in TiC_α depends on the deposition conditions, as well as post deposition treatment and the size of the crystallites. Stoichiometric composition in the Ti–C binary system allows variation of α in the range from 0.49 to 0.92 [23]. The mass density of bulk TiC is in the range 4.9–5.2 g cm^{-3}, which depends also on the composition. In our estimation, we assume the lowest value in this range to account for the nonequilibrium process of magnetron sputtering. The mass density of the a-C : H matrix can be estimated based on the IBA data from the ratio of the partial mass and partial volume of the matrix:

$$\rho_{CH} = \frac{m_{CH}}{V_{CH}} = \frac{(x - \alpha z)N_0 M_{CH} m_0}{(1 - zN_0 M_{TiC} m_0/\rho_{TiC})}, \qquad (8)$$

where $m_0 \approx 1.66 \times 10^{-24}$ g aem^{-1} is the mass of 1 aem. The resulting mass densities of the a-C : H matrix are plotted in figure 7 as a function of the H content in the matrix for two values of $\alpha = 1$ and 0.49 in TiC_α clusters. One can see that the uncertainty due to different α values is small. The error bars indicate mainly uncertainties in the components' concentrations. The mass density data for α=0.49 are also listed in table 1. One can see that the density varies between 1.5 and 1.9 g cm^{-3} and decreases as the H content increases.

6. Discussion

The outstanding mechanical, chemical and electrical properties of DLC are caused by the combination of sp^3 and sp^2 bonding in a certain ratio, as supported by x-ray photoelectron spectroscopy (XPS), and Raman and infrared (IR) spectroscopy [2, 24–26]. In order to evaluate whether the partial mass densities obtained above are reasonable we compare them with pure sp^3 and sp^2 bonded substances—crystalline diamond and graphite. The experimental DLC mass densities are lower than that of diamond (3.5 g cm^{-3}). Assuming the DLC matrix is a hydrogen-induced rearrangement of sp^3-bonds, the mass density of diamond-like hydrocarbonate (DLHC) due to the presence of hydrogen would vary according to the following simplified relation:

$$\rho_{DLHC} = \rho_D \cdot \left(1 - \left(1 - \frac{M_H}{M_C}\right)\frac{N_H^{DH}}{N_C^{DH} + N_H^{DH}}\right), \qquad (9)$$

where ρ_D is the density of diamond and N_C^{DH} and N_H^{DH} are the atomic densities of carbon and hydrogen in the DLHC matrix. The estimated density of DLHC as a function of the H content is shown in figure 7 by a solid line, where the ratios $N_H^{DH}/(N_C^{DH} + N_H^{DH})$ in equation (9) are equal to the values $N_H/(N_C + N_H - \alpha N_{Ti})$ on the abscissa.

Similarly, one can estimate the density of the C–H matrix by assuming H substitution of C-atoms in the sp^2 bonded graphite-like hydrocarbonate (GLHC). The density of graphite coatings significantly scatters from 1.6 to 2.27 g cm^{-3} due to the different growth techniques used [27]. Assuming the theoretical density of pure graphite $\rho_G = 2.27$ g cm^{-3}, the density of GLHC, ρ_{G-H}, as a function of the H content can be estimated by a corresponding substitution in equation (9) and is shown in figure 7 by a dashed line.

It follows that the mass densities of the a-C : H matrix are higher than those of GLHC in most of the cases. The only exception is the coating deposited at the floating substrate bias, which also shows a low atomic density of the a-C : H matrix attributed to an increased porosity formed under weak concurrent ion impingement.

It was shown that the mass density correlates with the fraction of sp^3 C–C and C–H bonding, both in hydrogen-free

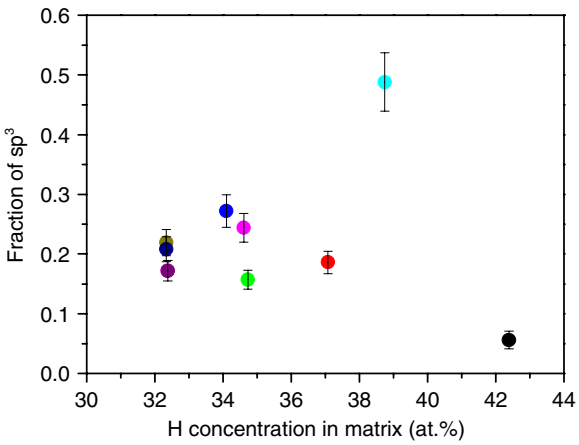

Figure 8. Estimated sp^3 fractions in the a-C : H matrix. The colours of the circles correspond to that in figure 7.

and hydrogenated DLC coatings with a constant H content [28, 29]. Comparing DLHC and GLHC mass densities with the estimated density ρ in equation (11) one can reasonably estimate the ratio of f_{sp^3} to f_{sp^2} fraction, taking into account the influence of the H content as described above. Assuming the experimental mass density is the weight average of the DLHC and GLHC mass densities, i.e.

$$\rho^{exp} = f_{sp^3} \cdot \rho_{DLHC} + f_{sp^2} \cdot \rho_{GLHC}, \tag{10}$$

one gets

$$f_{sp^3} = (\rho^{exp} - \rho_{GLHC})/(\rho_{DLHC} - \rho_{GLHC}) \tag{11}$$

and

$$f_{sp^2} = 1 - f_{sp^3}. \tag{12}$$

The f_{sp^3} fraction as a function of the H concentration estimated in such a way is plotted in figure 8 and is also listed in table 1. The absolute data of the f_{sp^3} fraction look reasonable for a-C : H coatings [1, 30]. The largest fluctuation of the sp^3 bonding fraction in the coating 100V80 (38.7 at% H) is most likely related to the fact that the highest volumetric fraction of TiC nanocrystallites corresponds to the smallest volumetric fraction of the a-C : H matrix and the highest volumetric fraction of the particle/matrix interface region. This likely increases the content of H–C bonds and thus the estimated sp^3 fraction in the matrix. It should be indicated that the hydrogen content measured by the IBA techniques includes both bonded and unbonded hydrogen, whose ratio may change due to the change in the ratio of deposition flux to impinging Ar^+ ions. Therefore, variation of the bonded/unbonded hydrogen ratio in the matrix may also contribute to the error in the sp^3 estimate.

7. Conclusions

The ability of IBA to provide concentration and depth profile of the chemical element is well known. It is also known that the ERD technique is the only direct and reliable method to give information about the concentration and depth profile of hydrogen in the film. Applying ERD as a quantitative method, we have shown that the hydrogen concentration is a function of both the flow rate of the C_2H_2 gas and the substrate bias voltage. This makes the correlation between the coating properties and only the gas flow rate rather questionable (for example, see [2]).

It has been demonstrated that IBA techniques are also very useful in evaluation of atomic and mass densities of a partial phase constituent. Such a possibility is of value in cases when other methods are lacking. In particular, the technique described can give the absolute atomic density of a composite coating and partial atomic densities of individual phases. Also, there is no other direct way to describe the mass density of the constituents, such as the a-C : H matrix of the composite coatings. These data can be used to describe the microstructure in more detail. Under certain assumptions we are able to obtain the sp^3 and sp^2 fractions in the matrix of the coatings.

Acknowledgments

The work is partially supported by the grant GK 02.513.11.3285 of the Russian Federal Agency on Science and Innovations and by the Netherlands Institute for Metals Research (NIMR). The work was performed in accordance with a cooperation agreement between the Skobeltsyn Institute of Nuclear Physics, Moscow State University, Russia, and the Department of Applied Physics, University of Groningen, The Netherlands.

References

[1] Robertson J 2002 *Mater. Sci. Eng.* R **37** 129
[2] Mikami T, Nakazawa H, Kudo M and Mashita M 2005 *Thin Solid Films* **488** 87
[3] Lanford W A, Trantvetter H P, Ziegler J F and Keller J 1976 *Appl. Phys. Lett.* **28** 566
[4] Grill A, Meyerson B, Patel V, Reimer J A and Petrich M A 1987 *J. Appl. Phys.* **61** 2874
[5] Doyle B L and Peercy P S 1979 *Appl. Phys. Lett.* **34** 812
[6] Turos A and Meyer O 1984 *Nucl. Instrum. Methods* B **4** 92
[7] Ingram D C, Woolam J A and Abbud G Bu 1986 *Thin Solid Films* **137** 255
[8] Long X, Peng X, He F, Liu M and Lin X 1992 *Nucl. Instrum. Methods* B **68** 266
[9] Avasthi D K, Kabiraj D, Mehta J, Mehta G K, Barshilia H C, Sah S, Mehta B R and Vankar V D 1995 *Vacuum* **46** 633
[10] Konishi Y, Konishi I, Sakauchi N, Hayashi S, Hirakimoto A and Suzuki J 1996 *Nucl. Instrum. Methods Phys. Res.* B **118** 312
[11] Wang W J, Wang T M and Chen B L 1996 *Nucl. Instrum. Methods Phys. Res.* B **117** 140
[12] Kudoyarova V Kh, Chernyshov A V, Zvonareva T K, Dzhelepova N B and Tsolov M B 1998 *Surf. Coat. Technol.* **100–101** 192
[13] Pei Y T, Galvan D and De Hosson J Th M 2005 *Acta Mater.* **53** 4505
[14] Pei Y T, Huizenga P, Galvan D and De Hosson J Th M 2006 *J. Appl. Phys.* **100** 114309
[15] Rigato V, Maggioni G, Boscarino D, Mariotto G, Bontempi E, Jones A H S, Camino D, Teer D and Santini C 1999 *Surf. Coat. Technol.* **116–119** 580
[16] Strondl C, Carvalho N M, De Hosson J Th M and Van der Kolk G J 2003 *Surf. Coat. Technol.* **162** 288
[17] Galvan D, Pei Y T and De Hosson J Th M 2005 *Acta Mater.* **53** 3925

[18] Mayer M 1999 *Proc. 15th Int. Conf. on the Application of Accelerators in Research and Industry (Denton, TX, 4–7 November 1998) AIP Conf. Proc.* **475** 541
[19] Doolittle L R 1985 *Nucl. Instrum. Methods Phys. Res.* B **9** 344
[20] Bohác V and Shirokov D M 1994 *Nucl. Instrum. Methods Phys. Res.* B **4** 497
[21] Chu W K, Mayer J W and Nicolet M A 1978 *Backscattering Spectrometry* (New York: Academic)
[22] Ziegler J F 1977 *Helium Stopping Powers and Ranges in all Elements* (Oxford: Pergamon)
[23] Massalski T B, Murray J L, Bennett L H and Baker H (ed) 1986 *Binary Alloy Phase Siagrams* (Metals Park, OH: ASM) p 595
[24] Lee K R, Kim M G, Cho S J, Eun K Y and Seong T Y 1997 *Thin Solid Films* **308** 263
[25] Thomas L, Ducarroir M, Hillel R and Berjoan R 2001 *Surf. Coat. Technol.* **142** 829
[26] Evans R D, Doll G L, Morrison P W, Bentley J, More K L and Glass J T 2002 *Surf. Coat. Technol.* **157** 197
[27] Kelly B T 1981 *Physics of Graphite* (London: Applied Science)
[28] Ferrari A C, Libassi A, Tanner B K, Stoloyan V, Yuan J, Brown L M, Rodil S E, Kleinsorge B and Robertson J 2000 *Phys. Rev.* B **62** 11089
[29] Kleber R, Jung K, Ehrhardt H, Muhling I, Breuer K, Metz H and Engelke F 1991 *Thin Solid Films* **205** 274
[30] Frauenheim Th, Blaudeck P, Stephan U and Jungnickel G 1993 *Phys. Rev.* B **48** 4823